2020-12-11

Locally monochromatic approximation to QED in intense laser fields

Heinzl, Thomas

http://hdl.handle.net/10026.1/17154

The locally monochromatic approximation to QED in intense laser fields

T. Heinzl,[1, *] B. King,[1, †] and A. J. MacLeod[1, ‡]

[1]Centre for Mathematical Sciences, University of Plymouth, Plymouth, PL4 8AA, United Kingdom
(Dated: December 17, 2020)

We derive an approximation to QED effects in intense laser fields which can be employed in laser-particle collisions. Treating the laser as a plane wave of arbitrary intensity, we split the wave into fast (carrier) and slow (envelope) modes. We solve the interaction dynamics exactly for the former while performing a local expansion in the latter. This yields a 'locally monochromatic' approximation (LMA), which we apply to nonlinear Compton scattering in circularly- and linearly-polarised backgrounds and to nonlinear Breit-Wheeler pair production. We provide the explicit link between the LMA and QED, and benchmark against exact QED results. The LMA is particularly useful for high-energy, intermediate-intensity collisions, where, unlike the 'locally-constant field' approximation, the LMA correctly describes the position and amplitude of harmonic features and exactly reproduces the low energy limit. We show that in the limit of high-intensity and large harmonic order, the locally-constant field approximation is recovered from the LMA.

I. INTRODUCTION

There is a growing interest in experimentally verifying the predictions of quantum electrodynamics (QED) in the strong field, high-intensity, regime. To access this regime in experiment, two requirements must be met: (i) an electromagnetic field is present which is sufficiently intense so that many field quanta participate in a given process; (ii) the momentum transfer (recoil) in scattering is large enough that the quantum nature of processes is manifest. Upcoming laser facilities such as ELI-Beamlines [1], ELI-NP [2], and SEL (see [3] for an overview) will reach field strengths to fulfil requirement (i). One way to fulfil (ii) is to use laser wakefield accelerated particles, recent successes of which include the generation of positron beams in the lab [4] and measurement of quantum signals of radiation reaction [5, 6].

Background electromagnetic field strength can be quantified using an intensity parameter, ξ, equivalent to the work done by the background over a Compton wavelength, in units of the background photon energy. When $\xi \sim O(1)$, the standard approach of treating the background in perturbation theory fails, because this assumes that processes are more probable when *fewer* background photons are involved. When $\xi \gg 1$, an alternative approximation is often employed, in which the instantaneous rate for processes in a constant ('crossed') plane wave background (treated without recourse to perturbation theory) is integrated over the classical trajectories of the scattered particles. This "locally-constant field approximation" (LCFA) [7–10] has the particular advantage that it can be applied to arbitrary external fields. Therefore, when used in conjunction with a classical Maxwell field equation solver, it can be employed in situations for inhomogeneous backgrounds. The locally-constant field

approximation is almost exclusively the method by which QED processes in intense fields are added to laser-plasma simulation codes [11–22]. It has recently been extended in several respects, by including higher derivative corrections [23–25], analysing simple, non-constant, fields in Schwinger pair production [26] and extending it to previously neglected processes [27, 28].

An alternative approach to probe the strong-field regime of QED is to use a conventional particle accelerator to fulfil the energy condition (ii), and a less intense laser to fulfil the field condition (i). This was demonstrated by the landmark E144 experiment [29] which investigated photon emission [30] and pair production [31, 32] in the weakly nonlinear regime. Using modern high-intensity laser systems, this form of experiment will be performed at E320 at FACET-II and at LUXE [33] at DESY, to measure QED in the highly nonlinear, non-perturbative regime, which was out of reach for E144. These experiments will access the intermediate intensity regime $\xi \sim O(1)$, where the locally-constant field approximation breaks down and fails to capture experimental observables such as the harmonic structure in spectra [34–36].

To address this problem we derive here, from QED, the "locally monochromatic approximation" (LMA). Because the LMA is based upon a perturbation around a monochromatic background, it is not suitable for intense laser-matter collisions where a plasma is generated. Instead, it *complements* the locally-constant-field approximation by covering the regime of high-energy and intermediate intensity where the LCFA becomes invalid. As usual, we assume that the laser background is well defined and backreaction [[37, 38] can be neglected to a first approximation. Rather than taking the constant crossed field result to be fundamental and the basis of the approximation, the LMA builds upon the monochromatic result, which is more specific to propagating fields such as laser pulses. One can show that both field configurations are 'null' (characterised by vanishing field invariants) and thus have the *same* degree of symmetry so that the dynamics becomes maximally super-integrable

in either case [39, 40].

Various numerical codes have already been implemented that include the QED effects of nonlinear Compton scattering and nonlinear Breit-Wheeler pair-creation, by using an "instaneously monochromatic" rate that samples a non plane-wave field around the probe particles. Examples include the simulation code to support the SLAC E144 experiment [29], CAIN [41] and IP Strong [42], which has lately been used to provide simulation support for the planning of the LUXE experiment [33].

In this paper, we formalise the LMA and identify the approximations necessary to derive it from QED. We find the LMA treats the fast dynamics related to the carrier frequency of the plane wave exactly, but uses a local expansion to describe the slow dynamics associated with the pulse envelope. This combines the slowly-varying envelope approximation [43–47] with the locally-constant field approximation, improving upon both. It captures features to which the locally-constant field approximation is blind, yet because it is still an explicitly local approximation, it can be added to single-particle simulation codes. Furthermore, by benchmarking the LMA against exact calculations in pulses, an additional feature in the mid-IR region of nonlinear Compton scattering will become apparent, which may provide an additional signal to be searched for in experiment.

The paper is organised as follows. In Sec. II we outline the key steps in deriving the LMA for a general first-order strong field QED process. In Sec. III we give an outline of the numerical methods that form the basis of our benchmarking against finite-pulse results. The LMA for nonlinear Compton scattering is then compared to QED in circularly and linearly polarised pulse backgrounds in Sec. IV. We demonstrate the validity of the LMA for nonlinear Breit-Wheeler pair production in Sec. V. We conclude in Sec. VI. In Appendix A, a detailed derivation of the LMA for nonlinear Compton scattering in a circularly polarised background is presented and in Appendix B we include an alternative derivation of the infra-red[1] limit of nonlinear Compton scattering, demonstrating also that the correct limit is trivially reproduced from the LMA. Finally, in Appendix C, we show that the locally-constant field approximation can be recovered as a high-intensity limit of the LMA.

II. OUTLINE OF THE LOCALLY MONOCHROMATIC APPROXIMATION

Let the gauge potential of the background, $a_\mu(\varphi)$, depend only on the phase $\varphi = k \cdot x$, with k being the wave four-vector. We will work in lightfront coordinates

---

[1] Here and throughout, we use 'infra-red' to denote low *lightfront* energy $n \cdot P$, for n the laser propagation direction and P any given particle momentum. This is a natural variable in plane wave calculations.

$x = (x^+, x^-, \boldsymbol{x}^\perp)$ where $x^\pm = x^0 \pm x^3$ and $\boldsymbol{x}^\perp = (x^1, x^2)$. Here x^+ is lightfront time while x^- and $\boldsymbol{x}^\perp$ are called the longitudinal and perpendicular directions, respectively [48]. With this notation, the wave vector of the background $k_\mu = \delta_\mu^+ k_+$, and $\varphi = k_+ x^+$. The scattering amplitude, S_{fi}, for an incoming electron with on-shell momentum p, $p^2 = m^2$, is then calculated using the Volkov wavefunction [49],

$$\Psi_p(x) = \left(1 + \frac{\not{k}\not{a}(\varphi)}{2k \cdot p}\right) u_p e^{-iS_p(x)} . \tag{1}$$

In the exponent, $S_p(x)$ is the classical action for an electron in a plane wave background,

$$S_p(x) = p \cdot x + \int_{-\infty}^{\varphi} \frac{2p \cdot a(t) - a^2(t)}{2k \cdot p} dt. \tag{2}$$

The scattering amplitude S_{fi} in a plane wave background can then be written as

$$S_{fi} = (2\pi)^3 \delta_{-,\perp}^3 (p_{\text{in}} - p_{\text{out}}) \mathcal{M}, \tag{3}$$

with an invariant amplitude $\mathcal{M}$. Due to the non-trivial structure of the background, overall momentum conservation (encoded in the delta functions) only holds in three directions, $\{-, \perp\}$.

A closed form solution for phase integrals such as (2) is only known for some special cases of the background field, for example infinite "monochromatic" plane waves (see e.g. [8] for extensive applications). Beyond these solutions, one can turn to a numerical approach or employ an approximation. The slowly varying envelope approximation is known to simplify the classical action (2) occurring in the exponent and hence make the phase integrations tractable [43–47]. It is applied as follows. Let the pulse $a_\mu(\varphi)$ have the form

$$a^\mu(\varphi) = m \xi f\left(\frac{\varphi}{\Phi}\right) \left(\varepsilon^\mu \cos\delta \cos\varphi + \bar{\varepsilon}^\mu \sin\delta \sin\varphi\right) , \tag{4}$$

where ξ is the dimensionless Lorentz and gauge invariant measure of the field intensity [50], $f(\varphi/\Phi)$ is the pulse envelope with phase duration Φ and ε^μ, and $\bar{\varepsilon}^\mu$ are polarisation directions satisfying $\varepsilon^2 = \bar{\varepsilon}^2 = -1$ and $\varepsilon \cdot \bar{\varepsilon} = k \cdot \varepsilon = k \cdot \bar{\varepsilon} = 0$. The parameter $\delta \in (0, \pi/2)$ determines the polarisation of the pulse; $\delta = 0$ for linear polarisation along ε, $\delta = \pi/2$ for linear polarisation along $\bar{\varepsilon}$ and $\delta = \pi/4$ for circular polarisation[2]. We consider the pulse envelope to be asymptotically switched on and off, $\lim_{\varphi \to \pm\infty} f(\varphi) = 0$.

The slowly varying envelope approximation assumes that the pulse duration Φ is sufficiently long that terms of order $\mathcal{O}(\Phi^{-1})$ can be neglected. (Higher orders can in principle be included in the approximation but they

---

[2] We make implicit a normalisation factor in the gauge potential (4) such that $\text{Max}[a_\mu(\varphi)/(m\xi)] = 1$.

will lead to a more complicated result that takes longer to numerically evaluate and, as we shall see, the leading order terms will already be sufficient to reproduce the main features of spectra.) As a result, derivatives of the envelope with respect to the phase can be neglected, because they are of the form $df(\varphi/\Phi)/d\varphi \sim \Phi^{-1}f'(\varphi/\Phi)$. In other words, the envelope varies slowly compared to the fast dynamics of the carrier frequency. The practical benefit of this is that we can simplify the classical action (2). More explicitly, the classical action will have terms both linear and quadratic in the field envelope. In all terms involving both fast and slow oscillations, we integrate by parts, picking up terms of order $\mathcal{O}(\Phi^{-1})$ which we neglect, and so remove the integrals from (2). This gives us, for the possible linear terms arising,

$$\int_{-\infty}^{\varphi} d\psi\, f\left(\frac{\psi}{\Phi}\right)\{\cos\psi, \sin\psi\} \simeq f\left(\frac{\varphi}{\Phi}\right)\{\sin\varphi, -\cos\varphi\},$$ (5)

and for the possible quadratic terms

$$\int_{-\infty}^{\varphi} d\psi\, f^2\left(\frac{\psi}{\Phi}\right)\{\cos^2\psi, \sin^2\psi\}$$
$$\simeq \frac{1}{2}f^2\left(\frac{\varphi}{\Phi}\right)\left\{(\varphi + \sin\varphi\cos\varphi), (\varphi - \sin\varphi\cos\varphi)\right\}.$$ (6)

For the particular case of a circularly polarised background, there arises a term containing only slow oscillations (the integral of f^2 without trigonometric functions), which must be approximated by different means (see below). With these approximations, the background-dependent parts of the classical action can always be put in the form

$$S_p(x) \simeq G\left(\varphi, \frac{\varphi}{\Phi}\right) + \frac{1}{2}\alpha\left(\frac{\varphi}{\Phi}\right)[u(\varphi) - u^{-1}(\varphi)]$$
$$+ \frac{1}{2}\beta\left(\frac{\varphi}{\Phi}\right)[v(\varphi) - v^{-1}(\varphi)].$$ (7)

The functions α and β are purely slowly-varying functions of the phase φ. The functions $u(\varphi)$ and $v(\varphi)$ are of the form $\exp(ic\varphi)$, for $c \in \{1, 2\}$. Note the similarity of the form of the exponent with the generating function for the Bessel function of the first kind,

$$\exp\left\{\tfrac{1}{2}z\left(\frac{\varphi}{\Phi}\right)[u(\varphi) - u^{-1}(\varphi)]\right\} = \sum_{n\in\mathbb{Z}} u^n(\varphi)J_n\left[z\left(\frac{\varphi}{\Phi}\right)\right].$$ (8)

This was recognised and exploited in [43] and essentially gives a generalisation of the infinite monochromatic field results [8, 51] to the case where the argument of the Bessel function now depends slowly on the phase. There will also appear rapidly oscillating terms in the pre-exponent, but these can be incorporated by differentiating (8) with respect to z and combining terms. The scattering amplitude will thus be defined in terms of harmonics, represented by the sum over integers n in (8).

So far everything has been typical for the application of the slowly-varying envelope approximation in the strong-field QED literature [43–47]. It is at this point that we

take the further step of performing a local expansion in the phase variables to arrive at a local "rate" which can be implemented in one-particle numerical simulations.

To define the local expansion, we will concentrate on single (dressed) vertex "one-to-two" processes: nonlinear Compton scattering and nonlinear Breit-Wheeler pair production. The amount of literature on these processes has become too large to be cited here in full; regarding nonlinear Compton scattering see [7, 52, 53] for the original papers, [8, 54] for reviews and [45, 55–58] for a selection of more recent results. Nonlinear Breit-Wheeler pair creation was first discussed in [7, 59, 60], while the study of finite size effects was initiated in [61]. Both processes were observed (at mildly nonlinear intensities) by the SLAC E144 experiment [29, 30, 32]. For the two examples to be considered, the reduced amplitude $\mathcal{M}$ in (3) will have one phase integral, and after applying the slowly-varying envelope approximation, will be defined in terms of an infinite sum over the harmonic order n, i.e.

$$\mathcal{M} = \sum_{n=-\infty}^{\infty} \int d\varphi\, \mathcal{M}_n(\varphi).$$ (9)

Squaring the amplitude for the probability, we will have something of the form,

$$\mathbb{P} \sim \sum_{n,n'=-\infty}^{\infty} \int d\Omega_{\text{LIPS}} \int d\varphi\, d\varphi'\, \mathcal{M}_n^\dagger(\varphi)\mathcal{M}_{n'}(\varphi'),$$ (10)

i.e., a double infinite sum over harmonic orders, two phase integrals, and an integration over the Lorentz invariant phase space of the process, $d\Omega_{\text{LIPS}}$.

Now we perform a local expansion of the probability, in analogy to the locally-constant field approximation (see e.g. [7–10]). We make a change of variables to the sum and difference of phases,

$$\phi = \frac{1}{2}(\varphi + \varphi'), \quad \theta = \varphi - \varphi'.$$ (11)

Terms in the probability are then expanded in a Taylor series in $\theta \ll 1$, and the slowly-varying envelope approximation is then applied to all derivatives of the pulse envelope, giving

$$f\left(\frac{\varphi}{\Phi}\right) \approx f\left(\frac{\varphi'}{\Phi}\right) \approx f\left(\frac{\phi}{\Phi}\right).$$ (12)

This allows the $d\theta$ integrals to be performed, and the probability takes the form

$$\mathbb{P} = \int d\phi\, \mathcal{R}(\phi),$$ (13)

where $\mathcal{R}(\phi)$ is interpreted as a local "rate"[3]. For the processes of nonlinear Compton scattering and nonlinear Breit-Wheeler pair production we can write:

$$\mathbb{P}_{\text{LMA}} \approx \int d\phi\, \mathcal{R}_{\text{mono}}[\xi f(\phi/\Phi)],$$ (14)

_____

[3] In general $\mathcal{R}(\phi)$ will contain infinite sums over harmonic orders,

where $\mathcal{R}_{\mathrm{mono}}$ is the probability per unit phase of the process in a monochromatic (infinitely long) plane wave. For a circularly polarised background the LMA is exactly equal to the integral on the right-hand side of (14). For a linearly polarised background, it is not so straightforward, as interference between different harmonic orders is included, but we will find that, to a good approximation, both sides of (14) are equal.

To conclude this outline of the LMA, we reiterate that the LMA is simply the application of two well-known approximations in the strong-field QED literature, the slowly varying envelope approximation and the "local" expansion in the relative phase variable, θ, carried out at the level of the probability. For each term in the local expansion we apply the slowly-varying envelope approximation, which reduces the complexity of the rates and allows us to progress further analytically. What this means is that no further restrictions have to be imposed on the pulse envelope beyond those required for the slowly-varying envelope approximation to be valid, i.e. that the phase duration Φ be sufficiently large that derivatives of the envelope can be safely neglected. Although the approximation has been used before for a circularly polarised background [62], as far as we are aware, this is the first explicit derivation and benchmarking with the direct calculation from QED for a plane-wave pulse. The monochromatic result is obtained from the LMA by taking the infinite pulse limit $\Phi \to \infty$, i.e. $f \to 1$.

III. DIRECT CALCULATION FROM QED FOR A PULSED BACKGROUND

We wish to benchmark the LMA against the numerical evaluation of exact expressions from high-intensity QED. We provide here the details of the integration scheme used. For both nonlinear Compton scattering and nonlinear Breit-Wheeler pair production in a plane-wave pulse, one can write the total probability in the form $\mathbb{P} = \alpha \mathcal{I}/\eta$, where α denotes the fine structure constant, $\eta = k \cdot P/m^2$ is the energy parameter of the incoming particle (where k is the light-like wave vector of the plane wave background, P is the four-momentum of the incoming particle) and $\mathcal{I}$ is a triple integral. $\mathcal{I}$ involves two phase integrals, ϕ, θ, and an integral over s, the fraction of the incoming particle's light-front momentum, P^-, carried away by the emitted particle. For nonlinear Compton
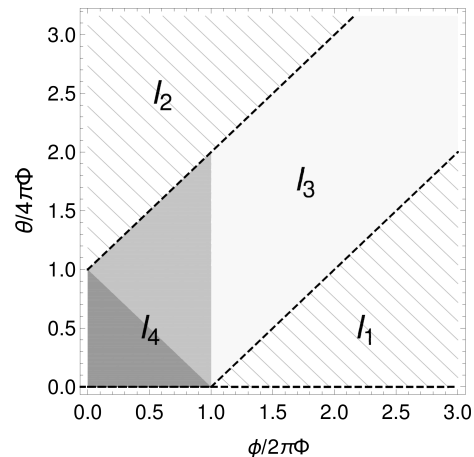
---

and a number of final state momentum integrals. The aim is to do as many of these final state momentum integrals as possible. Despite the added complexity which arises from retaining a slowly varying dependence on the phase variable ϕ, the number of final state integrals that can be performed is the same in the LMA as for a first order process in an infinite monochromatic plane wave [8, 51] (see appendix A).

FIG. 1. Overview of the regions integrated over in the ϕ-θ plane. The non-striped regions are inside of the pulse: $|\varphi'| < 2\pi\Phi$. The dark subregion in the area covered by I_4 signifies $|\varphi| < 2\pi\Phi$.

scattering, this is of the form:

$$\mathcal{I} = \int_{-\infty}^{\infty} \mathrm{d}\phi \int_0^1 \mathrm{d}s \left\{ -\frac{\pi}{2} \right.$$
$$\left. + \int_0^{\infty} \frac{\mathrm{d}\theta}{\theta} [1 + h(a, s)] \sin [g(s)\theta\mu(\phi, \theta)] \right\} . \quad (15)$$

For the numerical calculation of the exact QED result, we are using the "$i\epsilon$" regularisation at the level of the probability (see e.g. [63]), as evidenced by the $\pi/2$ counter-term in Eq. (15). The dependence on the field a defined in (4) resides in both $h(a, s)$ and in the Kibble mass [64, 65] normalised by the electron mass:

$$\mu(\phi, \theta) = 1 - \frac{1}{\theta} \int_{\phi-\theta/2}^{\phi+\theta/2} \frac{a^2}{m^2} + \left(\frac{1}{\theta} \int_{\phi-\theta/2}^{\phi+\theta/2} \frac{a}{m} \right)^2 .$$
$$(16)$$

In what follows we will outline some manipulations allowing for a straightforward numerical integration of $\mathcal{I}$.

The phase integration plane (ϕ, θ) can be split naturally into subregions where the integrand in (15) takes a specific form according to the following two observations: First, the field-dependent function $h(a, s)$ only has support for $a \neq 0$. Second, the Kibble mass becomes phase-independent when $\phi \pm \theta/2$ obey certain inequalities (see below).

Suppose we consider a pulse envelope, $f(\varphi/\Phi)$, which is symmetric about the origin with support $|\varphi| < L/2$. The example pulse shape we consider in this paper is $f = \cos^2$, where the phase duration is $L = \pi\Phi$ and the pulse length parameter, Φ, can be related to the number of cycles, N, via $\Phi = 2N$. Using the symmetry of the integrand, we only have to consider the first quadrant in the (ϕ, θ)-plane, which splits into the sub-regions shown in Fig. 1 such that $\mathcal{I} = \int ds \sum_{k=1}^4 I_k$.

To deal with the infinite numerical integation of a non-linearly oscillating pure phase term, we first rewrite the regularisation factor as

$$\frac{\pi}{2} = \int_0^\infty \frac{d\theta}{\theta}\,\sin K\theta,$$

which is independent of the choice of the constant factor K. In order to make for a simpler numerical evaluation, we choose $K = g(s)$, allowing us to combine it with the other infinite phase term in (15). (Other choices are useful in other circumstances, see for example [66] and (B1) in the appendix.) Using this trick, we find that the first integral vanishes,

$$I_1 = \int_{2\pi\Phi}^\infty d\sigma \int_0^{2(\phi-2\pi\Phi)} \frac{d\theta}{\theta}\{-\sin[g(s)\theta]$$
$$+\sin[g(s)\theta\mu(\phi,\theta)]\} = 0.$$

This can be shown by noting that $\lim_{a\to 0}\mu(\phi,\theta) = 1$, and in this phase region the pulse has no support. This is because terms depending on the potential, $a(\varphi)$, $a(\varphi')$ are zero unless:

$$|\varphi| = |\phi+\theta/2| < 2\pi\Phi \quad\text{or}\quad |\varphi'| = |\phi-\theta/2| < 2\pi\Phi.$$

In contrast, the integral I_2 over the region where the pulse is yet to pass through, is non-zero:

$$I_2 = \int_0^\infty d\phi \int_{2(2\pi\Phi+\phi)}^\infty \frac{d\theta}{\theta}\{-\sin[g(s)\theta]$$
$$+\sin[g(s)\theta\mu(\phi,\theta)]\} \neq 0.$$

Nevertheless, it may be calculated analytically by noting that the combination $\theta\mu(\phi,\theta)$ accumulates a constant total phase, $\theta\mu \to \theta + \theta_\infty$, when the probe particle traverses the pulse and continues to propagate in vacuum. Explicitly, one finds for both nonlinear Compton and Breit-Wheeler processes that $\theta_\infty = 3\pi c_\varepsilon \xi^2\Phi/2$, where $c_\varepsilon = 1$ ($c_\varepsilon = 1/2$) for a circularly (linearly) polarised background. This finally leads to

$$I_2 = 4\pi\Phi\sin X[\cos X\,\text{Ci}\,Y - \sin X\,\text{Si}\,Y$$
$$+\frac{\pi}{2}\sin X - \frac{1}{Y}\sin(X+Y)], \quad (17)$$

where $X = \theta_\infty g(s)/2$ and $Y = 4\pi\Phi g(s)$. This is related to recent studies of interference effects in a double-pulse background [67, 68].

The remaining integral, I_3, collects the contributions where the average phase ϕ is outside the pulse, while the phase difference θ is large enough that $\phi - \theta/2$ reaches back into the pulse,

$$I_3 = \int_{2\pi\Phi}^\infty d\phi \int_{2(\phi-2\pi\Phi)}^{2(\phi+2\pi\Phi)} \frac{d\theta}{\theta}\{-\sin[g(s)\theta]$$
$$+\sin[g(s)\mu(\phi,\theta)]\},$$

The integrand oscillates with a slowly decaying amplitude for $\phi > 2\pi\Phi$ outside the pulse. As the oscillations

are regular, they can be handled by using many data points. We also expect (and will show later) that contributions from outside the pulse are important mainly in the infra-red region of the spectrum, where we have an analytical expression for the limit.

Finally, I_4 is just the evaluation of the full integral in Eq. (15), for $\phi \in [0, 2\pi\Phi]$, $\theta \in [0, 2(2\pi\Phi+\phi)]$, i.e. "on top of" the pulse. As this is a well-defined, finite integration range, convergence can be assured by simply increasing the sampling resolution of the integrand.
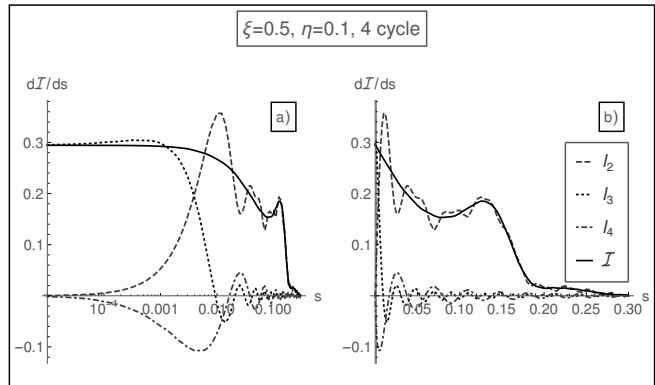

FIG. 2. A demonstrative plot showing how different parts of the integration region contribute to the spectrum (here, for a linearly polarised pulse) using a) a log scale and b) a linear scale.

The contribution of each part of the phase integration plane (ϕ,θ) to the spectrum is shown, for example parameters, in Fig. 2. This demonstrates that in the infra-red limit, $s \to 0$, the integral $\mathcal{I}$ from (15) is dominated by the sub-integral I_2, i.e. by contributions from phase regions located *outside* the pulse. On the one hand, this agrees with intuition based on the uncertainty principle—the lowest photon energies require the longest interaction of the electron with the background as has already been pointed out in the literature for nonlinear Compton scattering [9]. On the other hand, when studying the infra-red, one should take into account soft contributions from higher-order processes [63].

IV. NONLINEAR COMPTON SCATTERING

A. Circularly polarised plane wave

Having evaluated the full QED integrals for a pulse, we can now compare with the LMA. The latter is numerically more efficient, but also implies enhanced analytical control as it typically results in well-known special functions. Beyond these immediate advantages, our motivation to improve standard literature approximations is three-fold: (i) to have a locally defined rate which could in principle be implemented in numerical simulation codes; (ii) to be able to resolve the harmonic structures present in the exact QED probabilities with this ap-
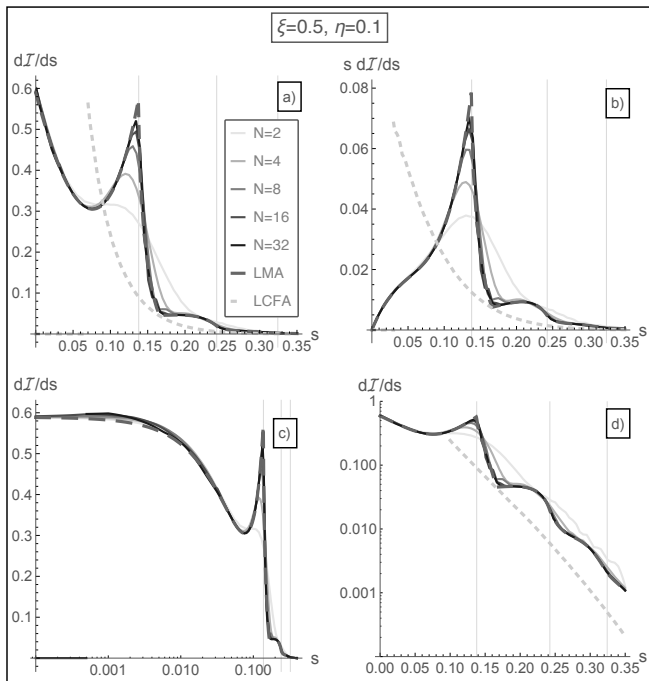
FIG. 3. The photon spectrum from nonlinear Compton scattering in a *circularly* polarised background, in the high-energy, weakly nonlinear regime, normalised by $N/2$ for pulses with different numbers of cycles, N. The locally-constant field approximation (light short-dashed line) poorly approximates the spectrum, whereas the LMA (dark long-dashed line) captures the harmonic structure and becomes more accurate as the length of the pulse increases. Plotted left-to-right is: a) the yield spectrum; b) the energy spectrum; c) the IR part of the spectrum (log-linear); d) the UV part of the spectrum (log). The vertical solid lines here and in the following figures correspond to the positions of the harmonic edges calculated for an infinite monochromatic plane wave.
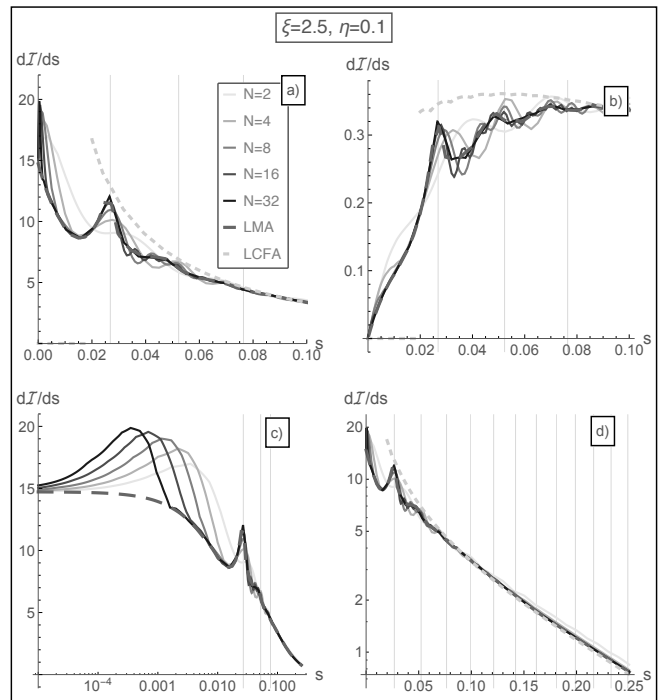
FIG. 4. The photon spectrum from nonlinear Compton scattering in a *circularly*-polarised background, in the high-energy nonlinear regime, normalised by half the number of laser cycles, $N/2$. The locally-constant field approximation (light short-dashed line) approximates the spectrum well for values of s corresponding to higher harmonics. The LMA (dark long-dashed line) captures both the harmonic structure and the large-s behaviour and becomes more accurate as the length of the pulse increases. Plotted left-to-right is: a) the yield spectrum; b) the energy spectrum; c) the IR part of the spectrum (log-linear); d) the UV part of the spectrum (log).

proximation; and (iii) to be able to work in the moderate intensity regime, $\xi \sim 1$, relevant for current state-of-the-art laser facilities. By construction, item (i) is readily provided by the LMA. To test the LMA for the other two goals, we will benchmark it against numerically integrated exact QED probabilities, beginning with the process of nonlinear Compton scattering.

Consider the interaction of an electron, initial invariant energy parameter $\eta_e = k \cdot p/m^2$, with the plane wave

$$a_\mu(\phi) = m\xi \cos^2\left(\frac{\phi}{\Phi}\right)\left(\varepsilon_\mu \cos\phi + \bar{\varepsilon}_\mu \sin\phi\right), \qquad (18)$$

which has circular polarisation and envelope $f \sim \cos^2$. The LMA to the nonlinear Compton spectrum in this setup is given in (A21). In Fig. 3 we compare the photon spectrum predicted by the LMA with the exact QED result, for the parameters $\xi = 0.5$ and $\eta_e = 0.1$, and various pulse lengths Φ. This is the low intensity, high-energy regime which will be probed at, for example, LUXE [33]. In this regime, the locally-constant field approximation, valid for $\xi^2/\eta_e \gg 1$ [69], is no longer applicable and fails

by a large margin as demonstrated in Fig. 3.

Each of the plots (a)–(d) in Fig. 3 shows the spectra for the LMA (dark long-dashed line), the locally-constant field approximation (light short-dashed line) and the numerically integrated exact QED results, the latter of which is plotted for various pulse lengths. (We recall the number of cycles N and the pulse duration Φ are related by $\Phi = 2N$.) The numerically integrated exact QED spectra have been normalised by $N/2$ to facilitate comparison. As discussed above, one of the steps in deriving the LMA for a given process is to first apply the slowly-varying envelope approximation, which assumes that the pulse duration is sufficiently long such that derivatives of the profile can be neglected. We can see the consequences of this in Fig. 3. As the pulse duration is increased, the LMA result remains the same (when normalised by pulse duration), but the results from the numerical integration of the exact QED probability become progressively more peaked around the first harmonic, and the agreement between this and the LMA improves. In all cases, the locally-constant field approximation completely misses not only the key harmonic structures and the infra-red

limit, but also fails in the high-energy, $s \to 1$, regime. This is characteristic of the locally-constant field approximation for $\xi < 1$.

Fig. 4 we show the same spectra as before, however for the increased field strength of $\xi = 2.5$. We are now in a regime where the locally-constant field approximation is able to more accurately capture at least the $s \to 1$ behaviour of the spectra, but we can see that the LMA is still vastly superior. In fact, in Fig. 4c we can distinguish three distinct regions of the spectrum on the interval $0 < s < 1$, defined in relation to the position of the first harmonic/Compton edge, which for a monochromatic plane wave is located at $s_1 = 2\eta_e/(1 + \xi^2 + 2\eta_e)$. There is the far infra-red sector where $0 < s \ll s_1$, the harmonic range where $s > s_1$ which includes all of the harmonic structure of the spectrum, and the intermediate regime where $s \lesssim s_1$. In both the far infra-red and the harmonic range the LMA gives a very good agreement with the numerically integrated exact QED spectrum, outperforming the locally-constant field approximation in both cases. One of the most striking improvements in this regard is the agreement between the LMA and the exact QED spectrum in the far infra-red, $s \to 0$ limit. This agreement is not only visible numerically; one can trivially derive the correct $s \to 0$ limit from the LMA, as shown in Appendix B where we also provide a novel derivation of the limit from the exact QED probability.

The second area in which the LMA performs well is in the harmonic range. For sufficiently long pulses, which in Fig. 4 corresponds to 8 cycles (full-width-half-max duration of around 11 fs for a 800 nm carrier wavelength), the LMA not only predicts the correct position of the leading harmonic in the spectrum, but is also accurate in predicting the locations and magnitudes of the sub-leading harmonics.

The only part of the spectrum in which the LMA deviates somewhat from the exact QED result is the intermediate regime where $s \lesssim s_1$. It turns out that this sector of the spectrum contains features which, to the best of our knowledge, have not been extensively commented on in the literature. Most numerical investigations of the exact QED spectrum/probability are compared to the locally-constant field approximation, which is well known (i) to not capture harmonic structure and (ii) to diverge towards the infra-red. The LMA, however, yields the correct infra-red limit, $s \to 0$, and very good agreement in the harmonic range, but does not capture the full structure of the spectrum in the intermediate range. In each of the spectra coming from the numerically integrated exact QED results there is a clear "bump" in the range just before the first harmonic. This same feature can be seen in various other works in the literature, see for example [23, 24, 70].

A qualitative explanation for these additional peaks is that a pulse profile introduces additional frequency scales in the dynamics, analogous to the usual harmonics found at locations determined by the carrier frequency scale of the background, see e.g. [45, 56, 57]. For the cur-

rent choice of a $\cos^2$ pulse envelope, we found that the approximate position of these peaks can be determined as follows. One first introduces a rescaled frequency, $\tilde{k}^0 = k^0/2I$, where k^0 is the carrier wave frequency and I is the integral[4] of the pulse profile, f. One then calculates the position of the first harmonic/Compton edge, s_1, using the rescaled energy parameter $\eta_e \to \eta_e/2I$. As pulse duration increases, the additional broad peaks get pushed further back into the infra-red and are smoothed out, eventually disappearing in the infinite plane wave (monochromatic) limit. Therefore an improvement of the accuracy of the LMA in this part of the spectrum might be achieved by including higher order terms in $1/\Phi$, i.e. the slowly-varying-envelope part of the approximation. The amplitude of these peaks also decreases significantly as ξ falls below unity.

Fig. 4 also shows that in the UV range, $s \to 1$, there is good agreement between the LMA and the locally-constant field approximation for $\xi = 2.5$. However, this is no longer true when $\xi = 0.5$ as in Fig. 3. To capture the UV limit in more detail one could adopt the methods of [71, 72] and use the saddle point method, noting that, in the exponent, the pre-factor of the Kibble mass is proportional to $(1 - s)^{-1}$. Following this route, though, is beyond the scope of our present discusion.

The case of a circularly polarised plane wave pulse gives the simplest form of the LMA due to the additional symmetries of the choice of background. The approach can, however, still be used for the case of linear polarisation, to which we now turn.

B. Linearly polarised plane wave

As above, we compare the LMA for a linearly polarised background field with the numerically integrated exact result for a fixed electron energy $\eta_e = 0.1$ and field strengths $\xi = 0.5$ (Fig. 5) and $\xi = 2.5$ (Fig. 6). In this case the LMA is given by (A34). Even for infinite monochromatic plane wave fields, the probability of nonlinear Compton scattering for a linearly polarised background field has extra structure compared to the circularly polarised case. The same is true for the LMA in a pulsed linearly polarised field. The source of the extra structure is that for linear polarisation the term which is quadratic in the background field in the classical action (2) is dependent on both the slow oscillations due to the pulse profile, and the fast oscillations of the carrier frequency of the plane wave. Within the LMA, this results in a non-trivial integration over the angular spread of the emitted photons. As a consequence (see Appendix A for details), there remains a double harmonic sum, compared to the circularly polarised case, where it simplifies

---

[4] For circular polarisation, i.e. the choice (18), one finds $I = \pi\Phi/2$. An analogous argument for linear polarisation (see below) employs the scaling $\tilde{k}^0 = k^0/\sqrt{2}\pi\Phi$.
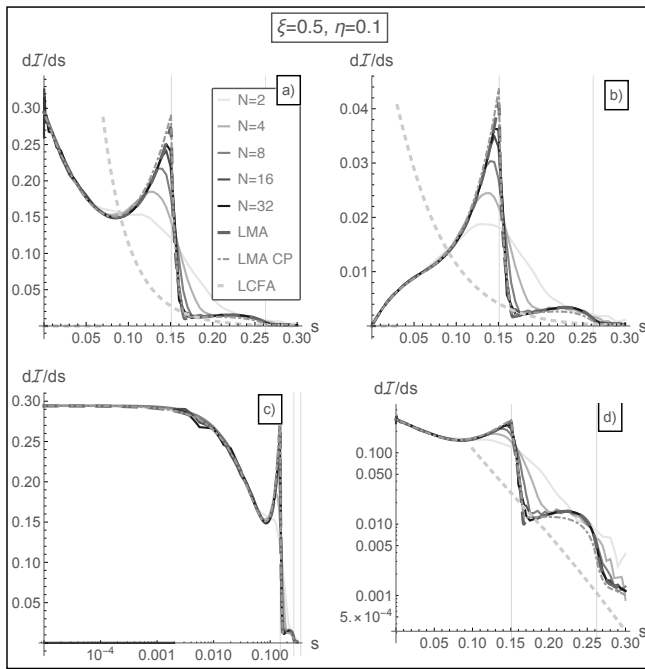
FIG. 5. The photon spectrum from nonlinear Compton scattering in a *linearly* polarised background, in the high-energy, weakly nonlinear regime, normalised by half the number of laser cycles, $N/2$. The agreement of the LMA (dark long-dashed line) and disagreement of the locally-constant field approximation (light short-dashed line) with the numerically exact results is similar to the circularly polarised case. The dot-dashed line is the spectrum acquired by taking the LMA for a *circularly* polarised background and rescaling the intensity parameter $\xi \to \xi/\sqrt{2}$.

due to the extra symmetry in the background. Hence, it is not possible to simply take the textbook expression for linearly polarised monochromatic plane waves [51] and localise the field intensity, $\xi \to \xi f$, as could be done in the circularly polarised case. In principle, the additional structure of a double-harmonic sum allows for the possibility of interference effects between the harmonics. However, in the intermediate intensity, high-energy regime, we did not find any appreciable contribution from this interference.

For weak fields, $\xi < 1$, the low-energy part of the spectrum, i.e. the region $s \lesssim s_1$ below the first harmonic, s_1, is well approximated by the perturbative contribution from the squared potential, a^2. In this case, the linearly polarised LMA turns out to be well-approximated by taking the circularly polarised LMA and making the replacement $\xi \to \xi/\sqrt{2}$, as is demonstrated in (6). Because of this, rescaling the circularly polarised result is a method which has been used to implement rates for linear polarisation in numerical codes.

However, this method fails for $\xi > 1$. In this regime, higher harmonics, proportional to a^{2n} for the nth harmonic, contribute to the spectrum and can no longer be obtained through a simple modification of the circularly

polarised LMA. This impact of the background polarisation at higher values of the field strength is demonstrated in Fig. 6. Although the position of the harmonics is still correctly predicted by the rescaled circularly polarised LMA, their amplitude is not, nor is the overall shape of the spectrum correctly captured: the rescaled circularly polarised result gives an underestimate for the smallest values of s, but an overestimate for larger values. Hence, the linearly polarised LMA proper, rather than the rescaled circularly polarised LMA, must be used in the intensity regime of upcoming experiments [33].

From both the circular and linear polarisation cases just discussed one notes that the higher the field strength ξ, the better the agreement between LMA and locally-constant field approximation in the ultra-violet (large-s) regime. In appendix C we show explicitly that this is not just some numerical accident. Indeed, we will derive the locally-constant field approximation as the high-field limit of the LMA.
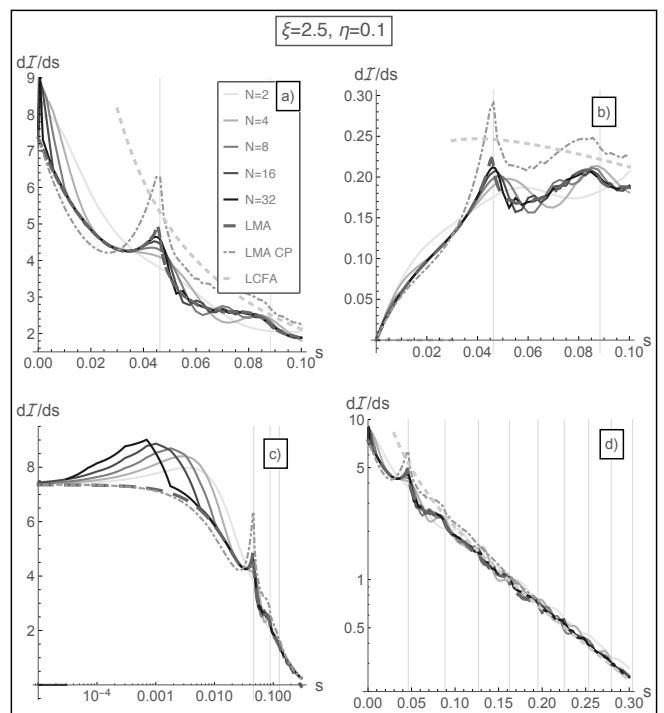

FIG. 6. The photon spectrum from nonlinear Compton scattering in a *linearly* polarised background, in the high-energy, nonlinear regime, normalised by half the number of laser cycles. The agreement of the LMA (dark long-dashed line) and the locally-constant field approximation (light short-dashed line) with the exact pulsed results is similar to the circularly polarised case. The dot-dashed line is the spectrum acquired by taking the LMA for a *circularly* polarised background and replacing the intensity parameter $\xi \to \xi/\sqrt{2}$. Unlike in the weak-field regime, the linearly polarised LMA is not well approximated by rescaling the intensity parameter in the circularly polarised LMA.

V. NONLINEAR BREIT-WHEELER

So far our focus has been on implementing and analysing the LMA for nonlinear Compton scattering. In principle, however, the LMA can be applied to any QED scattering process in a plane wave background. As another example, consider nonlinear Breit-Wheeler pair production, where an initial photon decays into an electron-positron pair. The derivation of the LMA for this process follows the same route as for nonlinear Compton scattering (see appendix A), and we again find that in the case of a circularly polarised plane wave the final differential probability is simply the textbook result in a monochromatic plane wave [51] with a localisation of the field strength, $\xi \to \xi f$, see (A36) in the appendix. A well known feature of the nonlinear Breit-Wheeler process is the strict lower bound, $n_\star$, on the harmonic number contributing for a given field strength and initial photon energy. This is because the outgoing particle states are massive, so that their production can only proceed above an energy threshold.

For a monochromatic plane wave, the lower bound is given by $n_\star^{mono} = 2(1 + \xi^2)/\eta_\gamma$, where $\eta_\gamma = k \cdot \ell/m^2$ is the energy parameter for the incident photon with four-momentum ℓ. Comparing this to (A37), we can see that for a pulse there are points along the phase for which the minimum harmonic $n_\star < n_\star^{mono}$ for the same ξ and η_γ.

At first glance, this would appear to mean that at the wings of the pulse, as $f \to 0$, the minimum harmonic contributing would decrease, and since Bessel harmonics of lower order are typically greater in magnitude, that the process would be more probable at lower field strengths. One has to keep in mind, though, that the argument $z(\phi)$ of the Bessel function depends on the pulse profile f and vanishes in the limit $f \to 0$. The only Bessel function surviving this limit is J_0. However, since the harmonic sum in (A36) is over strictly positive $n > 0$ and thus excludes J_0, there is no contribution to the probability for $f \to 0$. Hence, in comparison to nonlinear Compton scattering, the nonlinear Breit-Wheeler process will still require either very high field strengths, for which the locally-constant field approximation should be a good approximation, or very high initial photon energies.

For both the Compton and Breit-Wheeler processes, the momentum taken from the field increases with field strength, and the harmonic structure becomes less well defined. In order to demonstrate the LMA for the Breit-Wheeler process, the centre-of-mass energy should be close to the pair rest-energy in order that only very few laser photons are required for pair production to take place. In Fig. 7, we demonstrate such a situation, where we present the spectrum of electrons produced by a head-on collision of a 250 GeV photon ($\eta_\gamma = 3$) with a laser pulse of intensity $\xi = 1$. We note that the harmonic structure of the spectrum for long pulses is well-approximated by the LMA, whereas the locally-constant field approximation both misses the harmonics in the spectrum and under-predicts the yield.
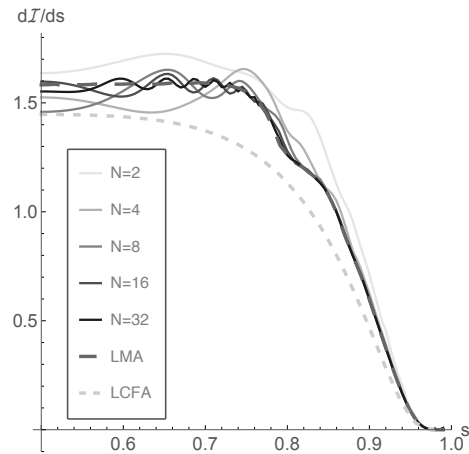

FIG. 7. The spectrum of electrons produced in nonlinear Breit-Wheeler pair production for $\xi = 1$, $\eta_\gamma = 3$. A comparison of the locally-constant field approximation (light short-dashed line) and the LMA (dark long-dashed line) with the exact numerical result in pulses of different numbers of cycles, N.

VI. SUMMARY

Motivated by the need to improve the theoretical tools required for supporting state-of-the-art laser experiments probing the high-intensity regime of QED, we have introduced here the locally monochromatic approximation (LMA).

This technique treats the quickly- and slowly-oscillating components of laser field profiles differently, in order to improve on the accuracy of the existing locally-constant field approximation, which essentially treats all field components as slowly varying. Oscillations due to the carrier frequency of the laser field are treated exactly, while the slowly-varying field envelope degrees of freedom are treated in a local expansion. Therefore, the accuracy of the LMA increases with increasing pulse duration as we have shown by comparing directly with exact QED results. This conclusion agrees with other works that have compared a train of monochromatic pulses with single short-pulse spectra [73, 74]. Although we have not included it here, the LMA could easily be extended to include a carrier-envelope-phase, since the separation between fast and slow time scales would remain (see e.g. [62] for an example of this applied to the slowly-varying-envelope approximation).

The LMA (or its precursors) have been used in several numerical codes, albeit in an ad-hoc fashion. To put the LMA on a firmer basis, we provide the first derivation from, and the first benchmarking against, QED in a plane wave background. In doing so we have identified the character of expansions at work and established how the accuracy improves with pulse duration. Finally, we have located spectral features in the mid-infra-red that are missed by this approximation.

We note, however, that despite being local in the phase

variable, the LMA is unsuitable for intense laser-matter interactions where plasma is present. This is because the LMA relies on the presence of structures particular to laser fields, essentially a central frequency and an envelope, which normally are absent in a plasma. Instead, the LMA can be thought to extend the LCFA up to higher energies and down to intermediate and low intensities, in situations where the background field is a laser pulse of well-characterised shape. Such a situation is to be found in upcoming high-energy experiments [33]. When applicable, the LMA correctly resolves harmonic structure in particle spectra. Whilst it is known that these can be washed out due to multi-particle effects [75], they have been observed in experiments [29, 35, 36, 76]. The washing-out effect is expected to be less significant if the electron beam has a narrow momentum spread. A further advantage of the LMA is its capability to capture the infra-red limit of nonlinear Compton scattering. In contrast, the locally-constant field approximation is well-known to fail in this regard.

In this paper we have considered the first-order processes of nonlinear Compton scattering and nonlinear Breit-Wheeler pair production, but the LMA could also be extended to higher-order processes such as trident pair production (see e.g. [77–82]) and double nonlinear Compton scattering (see e.g. [83–88]). This extension is not trivial, as it would need to deal with the appearance of resonant singularities in dressed propagators [89, 90] and is therefore a subject for further work.

Appendix A: Detailed derivation of the LMA

In Sec. II we presented only the key steps involved in calculating the LMA for a high-intensity QED process. To be more explicit, we turn to an example derivation for the process of nonlinear Compton scattering in a plane wave pulse. We will give a thorough account of the calculation for a circularly polarised pulse, and provide details about the technical differences in the linearly polarised case. We note that the calculation of the LMA for nonlinear Breit-Wheeler pair production discussed in Sec. V follows a completely analogous procedure. Hence, it will be sufficient to simply quote the final result below. Once the slowly-varying envelope approximation has been applied to the exponent of the scattering amplitude, the remaining analysis amounts to a generalisation of the calculation in a purely monochromatic plane wave (see for example [51] for the circularly polarised case).

Nonlinear Compton scattering is the process by which an electron of 4-momentum p scatters off a background plane wave pulse to emit a photon of momentum ℓ' and polarisation $\epsilon_{\ell'}^*$, $e^-(p) \to e^-(p') + \gamma(\ell')$. The amplitude is given by the standard S-matrix element

$$S_{\rm NLC} = -ie \int {\rm d}^4x \, \bar{\Psi}_{p'}(x) \slashed{\epsilon}_{\ell'}^* \Psi_p(x) e^{i\ell'\cdot x}. \quad (A1)$$

The explicit representation of the Volkov wavefunctions (1) and some trivial integrations lead to the representation (3) with reduced amplitude

$$\mathcal{M}_{\rm NLC} = -ie \int {\rm d}\varphi \, \mathcal{S}(\varphi) \exp\left(i\int_{-\infty}^\varphi \frac{\ell'\cdot\pi_p}{k\cdot(p-\ell')}\right). \quad (A2)$$

The integrand involves a spin structure

$$\mathcal{S}(\varphi) = \bar{u}_{p'}\left(1 + \frac{\slashed{a}(\varphi)\slashed{k}}{2k\cdot p'}\right)\slashed{\epsilon}_{\ell'}^*\left(1 + \frac{\slashed{k}\slashed{a}(\varphi)}{2k\cdot p}\right)u_p. \quad (A3)$$

and an exponential given in terms of the kinetic momentum of a classical electron in a plane wave background,

$$\pi_p^\mu(\varphi) = p^\mu - a^\mu(\varphi) + \frac{2p\cdot a(\varphi) - a^2(\varphi)}{2k\cdot p}k^\mu. \quad (A4)$$

We proceed now to the particular case of a circularly polarised pulse.

1. Circularly polarised plane wave pulse

The circularly polarised plane wave pulse is given by (4) with $\delta = \pi/4$ and a normalisation factor of $\sqrt{2}$ such that $\max(|a^\mu/m\xi|) = 1$,

$$a^\mu(\varphi) = m\xi f\left(\frac{\varphi}{\Phi}\right)\left(\varepsilon^\mu\cos\varphi + \bar{\varepsilon}^\mu\sin\varphi\right). \quad (A5)$$

The term quadratic in the gauge potential in (A4) only contains the slow timescale in φ:

$$a^2(\varphi) = -m^2\xi^2 f^2\left(\frac{\varphi}{\Phi}\right), \quad (A6)$$

and so the slowly-varying envelope approximation (5) need only be applied to the other terms linear in a^μ. This results in

$$\int_{-\infty}^\varphi \frac{\ell'\cdot\pi_p}{k\cdot(p-\ell')} \simeq G(\varphi) - \alpha_c\left(\frac{\varphi}{\Phi}\right)\sin\varphi + \alpha_s\left(\frac{\varphi}{\Phi}\right)\cos\varphi. \quad (A7)$$

The function $G(\varphi)$ is slowly varying with φ,

$$G(\varphi) = \frac{s}{2\eta_e(1-s)}\left[\left(1 + \frac{|\boldsymbol{\ell}'_\perp - s\boldsymbol{p}_\perp|^2}{s^2m^2}\right)\varphi + \int_{-\infty}^\varphi {\rm d}\psi\,\xi^2 f^2\left(\frac{\psi}{\Phi}\right)\right], \quad (A8)$$

and depends on $\eta_e = k \cdot p / m^2$, the normalised measure of the electron's light-front momentum, and $s = k \cdot \ell' / k \cdot p$, the light-front momentum fraction of the outgoing photon. The rapidly oscillating terms $\{\cos\varphi, \sin\varphi\}$ each have a slowly-varying pre-factor,

$$
\begin{aligned}
\alpha_c\left(\frac{\varphi}{\Phi}\right) &= \frac{\xi f(\frac{\varphi}{\Phi})}{\eta_e m (1-s)} (\ell' - sp) \cdot \varepsilon \ , \\
\alpha_s\left(\frac{\varphi}{\Phi}\right) &= \frac{\xi f(\frac{\varphi}{\Phi})}{\eta_e m (1-s)} (\ell' - sp) \cdot \bar{\varepsilon} \ ,
\end{aligned} \quad \text{(A9)}
$$

respectively, and depend on a 4-vector $\mathcal{L} = \ell' - sp$, projected onto the polarisation directions, ε and $\bar{\varepsilon}$, of the background. Defining an angle ϑ,

$$
\vartheta = \tan^{-1}\frac{\alpha_s}{\alpha_c} \ , \quad \text{(A10)}
$$

allows us to write

$$
\alpha_c\left(\frac{\varphi}{\Phi}\right) = z\left(\frac{\varphi}{\Phi}\right)\cos\vartheta \ , \qquad \alpha_s\left(\frac{\varphi}{\Phi}\right) = z\left(\frac{\varphi}{\Phi}\right)\sin\vartheta \ , \tag{A11}
$$

(we will use the shorthand $z(\varphi) \equiv z(\varphi/\Phi)$ in what follows) such that

$$
z(\varphi) = \sqrt{\alpha_c^2 + \alpha_s^2} = \sqrt{\frac{\xi^2 f^2(\frac{\varphi}{\Phi})}{\eta_e^2 m^2 (1-s)^2}|\ell' - sp|^2} \ . \tag{A12}
$$

This drastically simplifies the exponent (A7), and the reduced amplitude (A2), which becomes

$$
\mathcal{M}_{\mathrm{NLC}} = - ie \int \mathrm{d}\varphi \, \mathcal{S}(\varphi) \, e^{i\{G(\varphi) - z(\varphi)\sin(\varphi - \vartheta)\}}. \tag{A13}
$$

The probability is now calculated in the usual way by averaging/summing over incoming/outgoing spins and polarisations and integrating over the outgoing particle phase space with the result

$$
\begin{aligned}
\mathbb{P}_{\mathrm{NLC}}^{(\mathrm{circ})} =& \frac{\alpha}{16\pi^2 (k \cdot p)^2} \int \mathrm{d}\varphi \int \mathrm{d}\varphi' \int \frac{\mathrm{d}s}{s(1-s)} \int \mathrm{d}|\mathcal{L}_\perp|^2 \int \mathrm{d}\vartheta \, \mathcal{T}_{\mathrm{NLC}}(\varphi, \varphi') \\
& \times \exp\left[iG(\varphi) - iG(\varphi') - iz(\varphi)\sin(\varphi - \vartheta) + iz(\varphi')\sin(\varphi' - \vartheta)\right] \ .
\end{aligned} \tag{A14}
$$

Here, we have introduced the fine structure constant α and the auxiliary quantity

$$
\mathcal{T}_{\mathrm{NLC}}(\varphi, \varphi') = - 2m^2 + \left(1 + \frac{s^2}{2(1-s)}\right)\left(a(\varphi) - a(\varphi')\right)^2, \tag{A15}
$$

(up to a factor) representing the trace, $\mathrm{tr}\,\bar{\mathcal{S}}\mathcal{S}$, from the spin sum/average. For the perpendicular photon momentum integrals one has $\mathrm{d}^2\ell'_\perp = \mathrm{d}^2\mathcal{L}_\perp$ or, in polar coordinates,

$$
\int \mathrm{d}^2\ell'_\perp = \frac{1}{2}\int \mathrm{d}|\mathcal{L}_\perp|^2 \int \mathrm{d}\vartheta \ . \tag{A16}
$$

The trace term (A15) also depends on the gauge potential. However, the rapidly oscillating parts of both the exponential and the pre-exponential can always be combined into the Bessel generating function (8). Doing so, we expand each term in the probability into sums over Bessel harmonics, writing, in this expression, $z \equiv z(\varphi)$ and $z' \equiv z(\varphi')$,

$$
\mathcal{T}_{\mathrm{NLC}}(\varphi, \varphi')e^{-iz\sin(\varphi - \vartheta) + iz'\sin(\varphi' - \vartheta)} = \sum_{n,n'=-\infty}^{\infty} e^{-in\varphi + in'\varphi' + i(n-n')\vartheta}\left\{ -2m^2 J_n(z)J_{n'}(z') \right. \tag{A17}
$$

$$
\left. - m^2\xi^2\left(1 + \frac{s^2}{2(1-s)}\right)\left[\left(f^2\left(\frac{\varphi}{\Phi}\right) + f^2\left(\frac{\varphi'}{\Phi}\right)\right)J_n(z)J_{n'}(z') - f\left(\frac{\varphi}{\Phi}\right)f\left(\frac{\varphi'}{\Phi}\right)\left[J_{n+1}(z)J_{n'+1}(z') + J_{n-1}(z)J_{n'-1}(z')\right]\right]\right\} \ .
$$

Observe that the only dependence on the angle ϑ is through the term $\exp[i(n - n')\vartheta]$ (recall $G(\varphi)$ is also in-

dependent of ϑ, c.f. (A8)). The integral over this angle can then be performed, giving a δ-function which means

the probability only has support on $n = n'$, reducing the complexity from a doubly infinite sum to a single one. (It is interesting to note that in the calculation for a monochromatic plane wave [51] this factor setting $n = n'$ comes instead from a phase integral.)

The probability (A14) still has a complicated form, with two phase integrals and an integral over the transverse momentum variable $|\boldsymbol{\mathcal{L}}_\perp|^2$ which resides in the argument $z(\varphi)$ of the Bessel functions. As the integrals cannot be done analytically, the route forward now is to introduce a local expansion. We switch to the sum and difference variables (11) and expand in $\theta = \varphi - \varphi' \ll 1$, once again ignoring all derivatives of the field profile $f(\varphi/\Phi)$. Then we have $f(\varphi/\Phi) \approx f(\varphi'/\Phi) \approx f(\phi/\Phi)$, and consequently

$$z(\varphi) \approx z(\varphi') \approx z(\phi) \,, \qquad (A18)$$

(where we recall $\phi = (\varphi + \varphi')/2$). Finally, after setting $n = n'$ as discussed above, the remaining terms in the exponential are given by

$$
\begin{aligned}
&G(\varphi) - G(\varphi') - n\varphi + n'\varphi' \\
&= \left[\frac{s}{2\eta_e(1-s)} \left(1 + \frac{|\boldsymbol{\mathcal{L}}_\perp|^2}{s^2 m^2} + \xi^2 f^2\left(\frac{\phi}{\Phi}\right) \right) - n \right]\theta \,.
\end{aligned}
\tag{A19}
$$

The only dependence on the phase variable θ now comes from (A19), which appears in the exponent of the integrand. The integral over θ yields another δ-function, so

$$
\begin{aligned}
\mathbb{P}_{\mathrm{NLC}}^{(\mathrm{circ})} = -\frac{\alpha}{\eta_e} \int \mathrm{d}\phi \int \mathrm{d}s \int \mathrm{d}|\boldsymbol{\mathcal{L}}_\perp|^2 \sum_{n=-\infty}^{\infty} \delta\left(|\boldsymbol{\mathcal{L}}_\perp|^2 - m^2\left[2\eta_e(1-s)sn - s^2\left(1 + \xi^2 f^2\left(\frac{\phi}{\Phi}\right)\right) \right] \right) \\
\times \left\{ J_n^2\big(z(\phi)\big) + \frac{1}{2}\xi^2 f^2\left(\frac{\phi}{\Phi}\right)\left(1 + \frac{s^2}{2(1-s)}\right)\left[2J_n^2\big(z(\phi)\big) - J_{n+1}^2\big(z(\phi)\big) - J_{n-1}^2\big(z(\phi)\big) \right] \right\} \,.
\end{aligned}
\tag{A20}
$$

The remaining momentum integral is now trivial, giving the final result of

$$
\mathbb{P}_{\mathrm{NLC}}^{(\mathrm{circ})} \simeq -\frac{\alpha}{\eta_e} \int \mathrm{d}\phi \sum_{n=1}^{\infty} \int_0^{s_{n,*}(\phi)} \mathrm{d}s \left\{ J_n^2[z(\phi)] + \frac{1}{2}\xi^2 f^2\left(\frac{\phi}{\Phi}\right)\left(1 + \frac{1}{2}\frac{s^2}{(1-s)}\right)\left[2J_n^2[z(\phi)] - J_{n+1}^2[z(\phi)] - J_{n-1}^2[z(\phi)] \right] \right\} \,,
\tag{A21}
$$

in which

$$
z(\phi) = \frac{2n\xi\big|f\big(\frac{\phi}{\Phi}\big)\big|}{\sqrt{1 + \xi^2 f^2\big(\frac{\phi}{\Phi}\big)}} \left[\frac{s}{s_n(1-s)}\left(1 - \frac{s}{s_n(1-s)}\right) \right]^{1/2}
\tag{A22}
$$

and

$$
s_n = \frac{2n\eta_e}{1 + \xi^2 f^2\big(\frac{\phi}{\Phi}\big)} \,, \qquad \eta_e = \frac{k \cdot p}{m^2} \,, \qquad s = \frac{k \cdot \ell'}{k \cdot p}.
\tag{A23}
$$

(We have suppressed the argument of $s_n = s_n(\phi/\Phi)$ for brevity.) Momentum conservation leads to the condition $n \geq 1$ on the harmonic number, whereas kinematic considerations lead to a phase-dependent upper bound on the s-integration of $s_{n,*}(\phi) = s_n(\phi)/(1 + s_n(\phi))$. So for a circularly polarised plane wave field, (A5), the LMA gives a direct generalisation of the infinite monochromatic plane wave result (see e.g. [51]), where the field strength has been localised, i.e. turned into a function of phase, ϕ, by replacing $\xi \to \xi f(\phi/\Phi)$. As mentioned in the main text, this ad-hoc replacement has been used in the literature [62], but to the best of our knowledge, the necessary approximations required, and in fact the validity

of the approach, has not been studied. In [62] this trick of localising the field strength in the monochromatic result is also used for the case of a linearly polarised plane wave pulse. However, we will see below that the validity of this replacement may not be applicable in all cases.

2. Linearly polarised plane wave pulse

The derivation of the LMA for a linearly polarised plane wave pulse mostly follows the same path as for circular polarisation, and so we just point out the key differences, most importantly the reasons why it is not possible to simply take the standard results for the case of a linearly polarised monochromatic plane wave (see e.g. [8]) and "localise" the field strength ξ.

We will assume the pulse to be linearly polarised in the ε direction by adopting (4) with $\delta = 0$, hence

$$
a_\mu(\varphi) = m\xi f\left(\frac{\varphi}{\Phi}\right)\varepsilon_\mu \cos\varphi \,.
\tag{A24}
$$

Choosing a linearly polarised background leads to additional structure in the final expression for the probability.

The source of this is quite simple: in a circularly polarised pulse the term (A6) quadratic in the gauge potential is slowly-varying with φ, but in the linear case[5] contains rapidly oscillating parts,

$$a^2(\varphi) = -m^2 \xi^2 f^2\left(\frac{\varphi}{\Phi}\right) \cos^2 \varphi \; . \qquad (A25)$$

The appearance of the $\cos^2 \varphi$ term means that we must implement *both* slowly-varying envelope approximations, (5) and (6), for the linear terms. The exponent in (A2) is then

$$\int_{-\infty}^{\varphi} \frac{\ell' \cdot \pi_p}{k \cdot (p - \ell')} \simeq G(\varphi) - \alpha(\varphi) \sin \varphi + \beta(\varphi) \sin 2\varphi \; , \qquad (A26)$$

where we have introduced the function

$$G(\varphi) = \frac{s}{2\eta_e(1-s)} \left[\left(1 + \frac{|\ell'_\perp - s p_\perp|^2}{s^2 m^2}\right) + \frac{\xi^2}{2} f^2\left(\frac{\varphi}{\Phi}\right)\right] \varphi \; , \qquad (A27)$$

and the abbreviations

$$\alpha(\varphi) = \frac{\xi f\left(\frac{\varphi}{\Phi}\right)}{\eta_e m(1-s)} ((\ell' - sp) \cdot \varepsilon) \; ,$$

$$\beta(\varphi) = \frac{s}{8\eta_e(1-s)} \xi^2 f^2\left(\frac{\varphi}{\Phi}\right). \qquad (A28)$$

Notice that $\alpha(\cdot) \equiv \alpha_c(\cdot)$ (see (A9)) and thus depends on the projection of the photon momentum along ε,

but that $\beta(\varphi)$ is *independent* of the perpendicular directions. These simple observations have far reaching consequences. Most notably, the two trigonometric terms in (A26) cannot be combined as was done in (A13). Therefore, each of the oscillating terms in the exponential will have to be expanded individually, once they have been put into the form of the Bessel generating function (8). Furthermore, after implementing the expansion into Bessel harmonics, the probability will depend on terms like $J_n[\alpha(\varphi)]$, the argument of which depends on both the magnitude $|\mathcal{L}_\perp|$ and the angle ϑ (using the notation of the circularly polarised case). As such, only *one* of the two integrals coming from the perpendicular components of the outgoing photon momentum can be done, and the result will have a residual angular dependence (if one chooses to do the integral in $|\mathcal{L}_\perp|$). Remember that for circular polarisation the simple dependence on the angle ϑ in (A17) meant that the integral over ϑ could be performed, and the probability then only had support on $n = n'$. This is not the case for linear polarisation, and one finds that the number of harmonic sums cannot be reduced to the same amount as for the case of an infinite monochromatic plane wave.

With all this in mind we jump ahead to the probability, expand in the phase difference variable, $\theta = \varphi - \varphi'$. and perform all the remaining integrals which can be done analytically. Defining the combinations of Bessel functions

$$\Gamma_{0,n}(\phi) \equiv \sum_{r=-\infty}^{\infty} J_{n+2r}\left[\alpha(\phi)\right] J_r\left[\beta(\phi)\right] \; , \qquad (A29)$$

$$\Gamma_{1,n}(\phi) \equiv \frac{1}{2} \sum_{r=-\infty}^{\infty} \left\{J_{n+2r+1}\left[\alpha(\phi)\right] + J_{n+2r-1}\left[\alpha(\phi)\right]\right\} J_r\left[\beta(\phi)\right] \; , \qquad (A30)$$

$$\Gamma_{2,n}(\phi) \equiv \frac{1}{4} \sum_{r=-\infty}^{\infty} \left\{J_{n+2r+2}\left[\alpha(\phi)\right] + J_{n+2r-2}\left[\alpha(\phi)\right] + 2J_{n+2r}\left[\alpha(\phi)\right]\right\} J_r\left[\beta(\phi)\right] \; , \qquad (A31)$$

with arguments

$$\alpha(\phi) = -\frac{(n+n')\xi\left|f\left(\frac{\phi}{\Phi}\right)\right| \cos \vartheta}{\sqrt{1 + \frac{\xi^2}{2} f^2\left(\frac{\phi}{\Phi}\right)}} \sqrt{w_{n+n'}\left(1 - w_{n+n'}\right)}, \quad \beta(\phi) = \frac{\xi^2 f^2\left(\frac{\phi}{\Phi}\right)}{8\eta_e} \frac{s}{1-s} \qquad (A32)$$

and abbreviations

$$w_{n+n'} = \frac{s}{s_{n+n'}(1-s)} \; , \quad s_{n+n'} = \frac{(n+n')\eta_e}{1 + \frac{\xi^2}{2} f^2\left(\frac{\phi}{\Phi}\right)} \; , \qquad (A33)$$

————

[5] In the monochromatic limit, $f \to 1$, the use of linear polarisation is also well known to add some additional complexity to the probability as the quadratic term in a circularly polarised pulse is *constant*, while it varies with the phase in the linear case. Compare e.g. the results of [8] (linear) with [51] (circular) for nonlinear Compton scattering.

the probability for linearly polarised nonlinear Compton scattering finally becomes

$$\mathbb{P}_{\text{NLC}}^{(lin)} \simeq \frac{\alpha}{2\pi\eta_e} \int d\phi \sum_{n=1}^{\infty} \sum_{n'=1}^{\infty} \int_0^{s_{n+n',*}(\phi)} ds \int_0^{2\pi} d\vartheta \exp\left(-i(n-n')\phi\right)$$

$$\times \left\{ -\Gamma_{0,n}(\phi)\Gamma_{0,n'}(\phi) \right.$$

$$\left. -\frac{1}{2}\xi^2 f^2\left(\frac{\phi}{\Phi}\right)\left(1+\frac{s^2}{2(1-s)}\right)\left[\Gamma_{2,n}(\phi)\Gamma_{0,n'}(\phi)+\Gamma_{0,n}(\phi)\Gamma_{2,n'}(\phi)-2\Gamma_{1,n}(\phi)\Gamma_{1,n'}(\phi)\right]\right\}, \qquad (A34)$$

where the upper bound on the integration over s is given by, $s_{n+n',*}(\phi) = s_{n+n'}(\phi)/(1+s_{n+n'}(\phi))$.

Due to the additional structure and the infinite summations it is not possible to simply take the standard monochromatic plane wave result and "localise" the field strength, as could be done in the circularly polarised case. In principle, the appearance of this extra structure opens up the possibility of interference between different harmonics. However, in the parameter regime investigated in the main text we did not find a case where this interference was significant.

3. Nonlinear Breit-Wheeler Pair Production

Nonlinear Breit-Wheeler pair production [31, 32, 59] is the decay of a photon, of momentum ℓ and polarisation ε, into an electron-positron pair, with momenta p' and q' respectively: $\gamma(\ell) \to e^-(p') + e^+(q')$. In vacuum, this process is forbidden as it violates energy-momentum conservation, but here is made possible through the interaction with a background electromagnetic field. Again, the amplitude is given in terms of the Volkov wave functions (1), namely

$$S_{\text{BW}} = -ie\int d^4x\,\bar{\Psi}_{p'}(x)\slashed{\epsilon}_\ell\Psi_{-q'}(x)e^{-i\ell\cdot x}. \qquad (A35)$$

The derivation of the LMA is exactly the same as for nonlinear Compton scattering, and so we do not give any details here. Instead, we simply state the final result for the case of the circularly polarised plane wave (A5), namely

$$\mathbb{P}_{\text{BW}}^{(circ)} \simeq \frac{\alpha}{\eta_\gamma} \int d\phi \sum_{n>\lceil n_\star(\phi)\rceil}^{\infty} \int_{r_-(\phi)}^{r_+(\phi)} dr \left\{ J_n^2(z(\phi)) - \frac{1}{2}\xi^2 f^2\left(\frac{\phi}{\Phi}\right)\left(\frac{1}{2r(1-r)}-1\right)\left[2J_n^2(z(\phi))-J_{n+1}^2(z(\phi))-J_{n-1}^2(z(\phi))\right]\right\}$$

$$(A36)$$

where we have employed the abbreviations

$$z(\phi) = \frac{2n\xi\left|f\left(\frac{\phi}{\Phi}\right)\right|}{\sqrt{1+\xi^2 f^2\left(\frac{\phi}{\Phi}\right)}}\left[\frac{1}{r_n(1-r)r}\left(1-\frac{1}{r_n(1-r)r}\right)\right]^{1/2}, \quad r_n = \frac{2n\eta_\gamma}{1+\xi^2 f^2}, \quad \eta_\gamma = \frac{k\cdot\ell}{m^2}, \quad n_\star(\phi) = \frac{2(1+\xi^2 f^2(\phi))}{\eta_\gamma}.$$

$$(A37)$$

The lower bound on the harmonic number, $\lceil n_\star(\phi)\rceil$, is required by momentum conservation, as energy-momentum conservation must be satisfied when producing the outgoing pair. The kinematics of the nonlinear Breit-Wheeler process constrains the integration region to $r_-(\phi) < r < r_+(\phi)$, where $r_\pm = \frac{1}{2}\left(1 \pm \sqrt{1-n_\star(\phi)/n}\right)$.

Appendix B: Infra-red limit ($s \to 0$) of nonlinear Compton scattering

A well known discrepancy between the locally-constant field approximation and exact QED results is the failure of the former in the "infra-red", $s \to 0$, limit of the emitted photon spectrum. This is a consequence of performing a local expansion in $\theta = \varphi - \varphi' \ll 1$ for the entire pulse, whereas the low s spectrum is dominated by contributions from large θ [9]. Here we present a new derivation of this limit from the full QED probability in an arbitrary plane wave pulse, and show that the same

limit can be obtained trivially in the LMA.

The probability of nonlinear Compton scattering can be expressed in differential form as (see e.g. [23, 66]),

$$\frac{d\mathbb{P}_{\mathrm{NLC}}}{ds} = -\frac{\alpha}{\pi\eta_e} \int_{-\infty}^{\infty} d\phi \int_0^{\infty} d\theta \, \sin\left(\frac{\theta\mu}{2\eta_e}\frac{s}{1-s}\right) \left\{\frac{1}{\mu}\frac{\partial\mu}{\partial\theta} + \frac{g(s)}{\theta}\left[a(\phi+\theta/2) - a(\phi-\theta/2)\right]^2\right\}. \tag{B1}$$

Here we employ the Kibble effective mass μ introduced in (16) for the gauge potential $a_\mu = (0, \boldsymbol{a})$, whence

$$\mu(\phi, \theta) = 1 + \frac{1}{\theta}\int_{\phi-\theta/2}^{\phi+\theta/2} \boldsymbol{a}^2 - \left(\frac{1}{\theta}\int_{\phi-\theta/2}^{\phi+\theta/2} \boldsymbol{a}\right)^2. \tag{B2}$$

Rescaling the phase difference variable,

$$\theta = \frac{t}{s}, \tag{B3}$$

the Kibble effective mass (B2) becomes, to leading order

in small s,

$$\lim_{s\to 0} \mu \sim 1 + \frac{s}{t}\int_{-\infty}^{\infty} \boldsymbol{a}^2, \tag{B4}$$

which is independent of the phase variable ϕ. The derivative of the Kibble mass appearing in (B1) is then trivially of order s^2. Using also that, as $s \to 0$, $g(s) \to 1/2$, and replacing $1/(1-s) \to 1$ throughout, we find the leading order behaviour comes form the term in small square brackets in (B1), i.e. the squared difference of the potentials,

$$\frac{d\mathbb{P}_{\mathrm{NLC}}}{ds} \sim \frac{\alpha}{\pi\eta_e} \int_{-\infty}^{\infty} d\phi \int_0^{\infty} \frac{dt}{t} \, \sin\left(\frac{t}{2\eta_e}\right) \left[\boldsymbol{a}^2(\phi + t/2s) - \boldsymbol{a}(\phi + t/2s)\cdot\boldsymbol{a}(\phi - t/2s)\right], \tag{B5}$$

in which we have also shifted integration variables to compactify the expression. To proceed, we Fourier transform the gauge potentials, make use of

$$\int d\phi \, e^{i\omega(\phi+t/2s)}e^{i\nu(\phi\pm t/2s)} = 2\pi\delta(\omega+\nu)e^{it(\omega\mp\nu)/2s}, \tag{B6}$$

to get rid of the integral over ϕ, and put the differential probability in the form

$$\frac{d\mathbb{P}_{\mathrm{NLC}}}{ds} \sim \frac{\alpha}{2\pi^2\eta_e} \int d\omega \, \boldsymbol{a}(\omega)\cdot\boldsymbol{a}^\star(\omega)$$
$$\times \int_0^{\infty} \frac{dt}{t}\sin\left(\frac{t}{2\eta_e}\right)\left[1 - \cos\left(\frac{t\omega}{s}\right)\right]. \tag{B7}$$

The remaining integral over t can now be performed exactly,

$$\int_0^{\infty} \frac{dt}{t}\sin\left(\frac{t}{2\eta_e}\right)\left[1 - \cos\left(\frac{t\omega}{s}\right)\right]$$
$$= -\frac{\pi}{4}\left[-2 + \mathrm{sign}\left(1 - \frac{|\omega|}{s}\right) + \mathrm{sign}\left(1 + \frac{|\omega|}{s}\right)\right]. \tag{B8}$$

In the limit $s \to 0$ this yields

$$\lim_{s\to 0} \int_0^{\infty} \frac{dt}{t}\sin\left(\frac{t}{2\eta_e}\right)\left[1 - \cos\left(\frac{t\omega}{s}\right)\right] = \frac{\pi}{2}, \tag{B9}$$

so that the infra-red limit finally becomes

$$\lim_{s\to 0} \frac{d\mathbb{P}_{\mathrm{NLC}}}{ds} = \frac{\alpha}{4\pi\eta_e}\int d\omega \, \boldsymbol{a}(\omega)\cdot\boldsymbol{a}^\star(\omega). \tag{B10}$$

This agrees with the result found in [10].

Now, the locally-constant field approximation is well known to fail in predicting the correct value for the $s \to 0$ limit [9, 10, 23, 69, 70, 91, 92]. We have demonstrated in the main text that, on the other hand, the LMA gives a perfect match to the exact QED results numerically. It turns out that in the LMA, recovering the correct limit (B10) is completely trivial.

First consider the LMA of nonlinear Compton scattering in a circularly polarised plane wave pulse (A21). The argument of the Bessel functions $z(\phi)$, defined in (A22), has leading order behaviour $z(\phi) \to 0$ in the $s \to 0$ limit. In the $z \to 0$ limit, the Bessel functions obey,

$$\lim_{z\to 0} J_m(z) = \begin{cases} 1 & \text{for } m = 0 \\ 0 & \text{for } m \neq 0 \end{cases}. \tag{B11}$$

So the only term that remains non-zero in the $s \to 0$ limit is the term $\propto J_{n-1}^2(z)$ in (A21), with $n = 1$. Then, after Fourier transforming the remaining terms and calculating the resulting trivial integrals, one recovers precisely (B10). The same argument carries through for linear polarisation as well.

Appendix C: High-field limit ($\xi \gg 1$) of the LMA

We noted in the main text that the locally-constant field approximation can be derived as the high-field limit of the LMA; we show this explicitly here. We will focus on the simplest case, nonlinear Compton scattering in a circularly polarised background field, c.f. (A21).

We begin by considering the behaviour of the argument of the Bessel function (A22) for $\xi \gg 1$ which should be real and positive. For a particular value of the light-front momentum fraction, s, there is a minimum value of the harmonic number given by

$$n_{\min} = \frac{\bar{\xi}^3}{2\chi_e} \frac{s}{1-s} \left[1 + \frac{1}{\bar{\xi}^2} \right] , \qquad (C1)$$

where we use the shorthand $\bar{\xi} = \xi f$ and defined $\chi_e = \bar{\xi}\eta_e$.

We note that as $\bar{\xi} \to \infty$, $n \sim \bar{\xi}^3/\chi_e$, and hence the corresponding harmonic order at a fixed value of s becomes very large. In this limit, the behaviour of the Bessel function terms may be determined as follows. Let $v = s/s_{n,*}$ where $s_{n,*} = s_n/(1+s_n)$ is the edge of the nth harmonic. This removes any dependency on n from the s integration range:

$$\int_0^{s_{n,*}} \mathrm{d}s \to s_{n,*} \int_0^1 \mathrm{d}v.$$

Then the argument of the Bessel functions becomes:

$$z = \frac{2n\bar{\xi}}{\sqrt{1+\bar{\xi}^2}} \left[\frac{s_{n,*}}{s_n} \frac{v}{1-vs_{n,*}} \left(1 - \frac{s_{n,*}}{s_n} \frac{v}{1-vs_{n,*}} \right) \right]^{1/2} . \qquad (C2)$$

Recalling that $s_n = 2n\eta_e/(1+\bar{\xi}^2)$, we see that, in the limit of $\bar{\xi} \to \infty$, keeping all other variables fixed, $z \to n\zeta(v)$, where ζ is independent of n. In the high-field limit, $\bar{\xi} \gg 1$, the function $\zeta(v)$ tends to

$$\lim_{\bar{\xi} \gg 1} \zeta(v) \simeq 2 \left[v(1-v) \right]^{1/2} . \qquad (C3)$$

In this limit, the main contribution to the probability comes from the vicinity of $\zeta \sim 1$ or $v \sim 1/2$. In other words, the main contribution comes from the region where $z \sim n$. Using the high field limit of n, the argument of the Bessel functions, z, can be shown to approach the finite value

$$z \to \frac{\bar{\xi}^3}{\chi_e} \frac{s}{1-s} . \qquad (C4)$$

To proceed we follow the approach of Ritus [8] and introduce a new parameter,

$$\tau = \frac{\bar{\xi}}{2} \left[\left(\frac{z\chi_e}{\bar{\xi}^3} \frac{(1-s)}{s} \right)^2 - 1 \right] , \qquad (C5)$$

which characterises the difference between z and its limiting high-field value at the points of maximum contribution to the probability (with a normalisation set for later convenience). Then, using the relationship between z and the harmonic number n, we can express n in terms of τ,

$$n = \frac{\bar{\xi}^3}{2\chi_e} \frac{s}{1-s} \left(1 + \frac{2\tau}{\bar{\xi}} \right) + n_{\min} . \qquad (C6)$$

In the probability one now exchanges the order of summation (over n) and integration (over s). In the high-field limit, one can replace the summation by an integration over τ such that,

$$\mathbb{P}_{\mathrm{NLC}} \simeq -\frac{\alpha}{\eta_e} \int \mathrm{d}\phi \int_0^\infty \mathrm{d}s \int_{-\bar{\xi}/2}^\infty \mathrm{d}\tau \left(\frac{\bar{\xi}^2}{\chi_e} \frac{s}{1-s} \right) \left\{ J_n^2(n\zeta) - \bar{\xi}^2 \left(1 + \frac{1}{2} \frac{s^2}{(1-s)} \right) \left[\frac{1-\zeta^2}{\zeta^2} J_n^2(n\zeta) + J_n'^2(n\zeta) \right] \right\} . \qquad (C7)$$

As noted previously, in the high field limit, the minimum value $n_{\min}$ for the harmonic number becomes large, and the main contribution to the probability comes from the regions where $\zeta \sim 1$. These two conditions allow us to use the Watson representation [93] of the Bessel functions,

$$J_n(n\zeta) \simeq \left(\frac{2}{n} \right)^{1/3} \mathrm{Ai}(y) , \qquad y = \left(\frac{n}{2} \right)^{2/3} \left(1 - \zeta^2 \right) , \qquad (C8)$$

where $\mathrm{Ai}(y)$ is an Airy function. Implementing the Watson representation, expanding around $\bar{\xi} \gg 1$ and defining $u = s/(1-s)$ we can approximate

$$y \simeq \left(\frac{u}{2\chi_e} \right)^{2/3} (1 + \tau^2), \qquad (C9)$$

such that the probability turns into

$$\mathbb{P}_{\text{NLC}} \simeq -\frac{2\alpha}{\eta_e} \int \mathrm{d}\phi \int_0^\infty \frac{\mathrm{d}u}{(1+u)^2} \int_0^\infty \mathrm{d}\tau \left(\frac{u}{\chi_e}\right)^{1/3} \left\{ \text{Ai}^2(y) - \left(\frac{2\chi_e}{u}\right)^{2/3} \left(1 + \frac{1}{2}\frac{u^2}{(1+u)}\right) \left[y\text{Ai}^2(y) + \text{Ai}'^2(y)\right] \right\} .$$

$$(\text{C10})$$

In (C10) we made use of the fact that the only dependence of the probability on τ is through (C9), and so the integration in τ is symmetric in the $\bar{\xi} \gg 1$ limit.

Next, we change variables to $T = (u/2\chi_e)^{2/3}\tau^2$, use

the two Airy function identities [8, 93]

$$y\text{Ai}^2(y) + \text{Ai}'^2(y) = \frac{1}{2}\frac{\mathrm{d}^2}{\mathrm{d}y^2}\text{Ai}^2(y) , \qquad (\text{C11})$$

$$\int_0^\infty \frac{\mathrm{d}T}{\sqrt{T}}\text{Ai}^2(A+T) = \frac{1}{2}\int_{2^{2/3}A}^\infty \mathrm{d}x\text{Ai}(x) , \qquad (\text{C12})$$

and define

$$\bar{z} = \left(\frac{u}{\chi_e}\right)^{2/3} \qquad \text{Ai}_1(\bar{z}) = \int_{\bar{z}}^\infty \mathrm{d}x\text{Ai}(x) , \qquad (\text{C13})$$

to cast the probability into the form

$$\mathbb{P}_{\text{NLC}} \simeq -\frac{\alpha}{\eta_e} \int \mathrm{d}\phi \int_0^\infty \frac{\mathrm{d}u}{(1+u)^2} \left\{ \text{Ai}_1(\bar{z}) + \frac{2}{\bar{z}}\left(1 + \frac{1}{2}\frac{u^2}{(1+u)}\right)\text{Ai}'(\bar{z}) \right\} \qquad (\text{C14})$$

Finally, changing variables back to $s = u/(1+u)$ the probability can be put in the form

$$\mathbb{P}_{\text{NLC}} \simeq -\frac{\alpha}{\eta_e} \int \mathrm{d}\phi \int_0^1 \mathrm{d}s \left\{ \text{Ai}_1(\bar{z}) + \left(\frac{2}{\bar{z}} + s\chi\sqrt{\bar{z}}\right)\text{Ai}'(\bar{z}) \right\} \qquad (\text{C15})$$

This is *exactly* the locally-constant field approximation, cf. (A.14) of [23], where $\chi_\gamma \equiv s\chi$. Hence, the locally-constant field approximation is nothing but the high-field limit of the more general LMA which has been the subject of the present paper.

[1] Extreme Light Infrastructure – Beamlines (ELI-Beams), URL https://www.eli-beams.eu/.

[2] Extreme Light Infrastructure – Nuclear Physics (ELI-NP), URL https://www.eli-np.ro/.

[3] C. N. Danson, C. Haefner, J. Bromage, T. Butcher, J.-C. F. Chanteloup, E. A. Chowdhury, A. Galvanauskas, L. A. Gizzi, J. Hein, D. I. Hillier, et al., High Power Laser Science and Engineering **7**, e54 (2019).

[4] G. Sarri et al., Nature Communications **6**, 6747 (2015).

[5] J. M. Cole et al., Phys. Rev. X **8**, 011020 (2018), 1707.06821.

[6] K. Poder et al., Phys. Rev. X **8**, 031004 (2018), 1709.01861.

[7] A. I. Nikishov and V. I. Ritus, Sov. Phys. JETP **19**, 529 (1964), [Zh. Eksp. Teor. Fiz. **46**, 776 (1964)].

[8] V. I. Ritus, Journal of Soviet Laser Research **6**, 497 (1985), ISSN 1573-8760, URL https://doi.org/10.1007/BF01120220.

[9] C. N. Harvey, A. Ilderton, and B. King, Phys. Rev. A **91**, 013822 (2015), URL https://link.aps.org/doi/10.1103/PhysRevA.91.013822.

[10] A. Di Piazza, M. Tamburini, S. Meuren, and C. H. Keitel, Phys. Rev. A **98**, 012134 (2018), 1708.08276.

[11] E. N. Nerush, I. Y. Kostyukov, A. M. Fedotov, N. B. Narozhny, N. V. Elkina, and H. Ruhl, Phys. Rev. Lett. **106**, 035001 (2011).

[12] N. V. Elkina et al., Phys. Rev. ST Accel. Beams **14**, 054401 (2011).

[13] C. P. Ridgers et al., Phys. Rev. Lett. **108**, 165006 (2012).

[14] B. King, N. Elkina, and H. Ruhl, Phys. Rev. A **87**, 042117 (2013).

[15] S. S. Bulanov, C. B. Schroeder, E. Esarey, and W. P. Leemans, Phys. Rev. A **87**, 062110 (2013), 1306.1260.

[16] C. Ridgers, J. G. Kirk, R. Duclous, T. Blackburn, C. Brady, K. Bennett, T. Arber, and A. Bell, Journal of Computational Physics **260**, 273 (2014).

[17] A. Gonoskov, S. Bastrakov, E. Efimenko, A. Ilderton, M. Marklund, I. Meyerov, A. Muraviev, A. Sergeev,

I. Surmin, and E. Wallin, Phys. Rev. E **92**, 023305 (2015), 1412.6426.

[18] T. G. Blackburn, C. P. Ridgers, J. G. Kirk, and A. R. Bell, Phys. Rev. Lett. **112**, 015001 (2014), URL https://link.aps.org/doi/10.1103/PhysRevLett.112.015001.

[19] E. Gelfer, A. Mironov, A. Fedotov, V. Bashmakov, E. Nerush, I. Y. Kostyukov, and N. Narozhny, Physical Review A **92**, 022113 (2015).

[20] M. Jirka, O. Klimo, S. V. Bulanov, T. Z. Esirkepov, E. Gelfer, S. S. Bulanov, S. Weber, and G. Korn, Phys. Rev. E **93**, 023207 (2016), URL https://link.aps.org/doi/10.1103/PhysRevE.93.023207.

[21] A. Gonoskov, A. Bashinov, S. Bastrakov, E. Efimenko, A. Ilderton, A. Kim, M. Marklund, I. Meyerov, A. Muraviev, and A. Sergeev, Phys. Rev. X **7**, 041003 (2017), URL https://link.aps.org/doi/10.1103/PhysRevX.7.041003.

[22] E. S. Efimenko, A. V. Bashinov, A. A. Gonoskov, S. I. Bastrakov, A. A. Muraviev, I. B. Meyerov, A. V. Kim, and A. M. Sergeev, Phys. Rev. E **99**, 031201 (2019), URL https://link.aps.org/doi/10.1103/PhysRevE.99.031201.

[23] A. Ilderton, B. King, and D. Seipt, Phys. Rev. A **99**, 042121 (2019), 1808.10339.

[24] A. Di Piazza, M. Tamburini, S. Meuren, and C. H. Keitel, Phys. Rev. A **99**, 022125 (2019), 1811.05834.

[25] B. King (2019), 1908.06985.

[26] I. A. Aleksandrov, G. Plunien, and V. M. Shabaev, Phys. Rev. D **99**, 016020 (2019), 1811.01419.

[27] A. Ilderton, B. King, and A. J. Macleod, Phys. Rev. D **100**, 076002 (2019), 1907.12835.

[28] S. Tang, A. Ilderton, and B. King, Phys. Rev. A **100**, 062119 (2019), 1909.01141.

[29] C. Bamber et al., Phys. Rev. D **60**, 092004 (1999).

[30] C. Bula et al. (E144), Phys. Rev. Lett. **76**, 3116 (1996).

[31] G. Breit and J. A. Wheeler, Phys. Rev. **46**, 1087 (1934).

[32] D. Burke et al., Phys. Rev. Lett. **79**, 1626 (1997).

[33] H. Abramowicz et al. (2019), 1909.00860.

[34] S.-y. Chen, A. Maksimchuk, and D. Umstadter, Nature **396**, 653 (1998).

[35] Y. Sakai, I. Pogorelsky, O. Williams, F. O'Shea, S. Barber, I. Gadjev, J. Duris, P. Musumeci, M. Fedurin, A. Korostyshevsky, et al., Phys. Rev. ST Accel. Beams **18**, 060702 (2015), URL https://link.aps.org/doi/10.1103/PhysRevSTAB.18.060702.

[36] K. Khrennikov, J. Wenz, A. Buck, J. Xu, M. Heigoldt, L. Veisz, and S. Karsch, Phys. Rev. Lett. **114**, 195003 (2015), URL https://link.aps.org/doi/10.1103/PhysRevLett.114.195003.

[37] D. Seipt, T. Heinzl, M. Marklund, and S. S. Bulanov, Phys. Rev. Lett. **118**, 154803 (2017), URL https://link.aps.org/doi/10.1103/PhysRevLett.118.154803.

[38] R. Ekman and A. Ilderton (2020), 2002.03759.

[39] T. Heinzl and A. Ilderton, Phys. Rev. Lett. **118**, 113202 (2017), 1701.09166.

[40] T. Heinzl and A. Ilderton, J. Phys. A **50**, 345204 (2017), 1701.09168.

[41] K. Yokoya, *User's manual of CAIN version 2.35*, KEK Pub 4/96 ((2003)).

[42] A. Hartin, International Journal of Modern Physics A **33**, 1830011 (2018), https://doi.org/10.1142/S0217751X18300119, URL https://doi.org/10.1142/S0217751X18300119.

[43] N. B. Narozhnyi and M. S. Fofanov, J. Exp. Theor. Phys. **83**, 14 (1996), [Zh. Eksp. Teor. Fiz. **110**, 26 (1996)].

[44] K. McDonald (1997), www.hep.princeton.edu/ mcdonald/examples/gaussian2.pdf.

[45] D. Seipt and B. Kämpfer, Phys. Rev. A **83**, 022101 (2011), 1010.3301.

[46] D. Seipt, S. G. Rykovanov, A. Surzhykov, and S. Fritzsche, Phys. Rev. A **91**, 033402 (2015), 1412.2659.

[47] D. Seipt, V. Kharin, S. Rykovanov, A. Surzhykov, and S. Fritzsche, J. Plasma Phys. **82**, 655820203 (2016), 1601.00442.

[48] T. Heinzl, Lect. Notes Phys. **572**, 55 (2001), hep-th/0008096.

[49] D. M. Wolkow, Z. Phys. **94**, 250 (1935).

[50] T. Heinzl and A. Ilderton, Opt. Commun. **282**, 1879 (2009), 0807.1841.

[51] V. B. Berestetskii, E. M. Lifshitz, and L. P. Pitaevskii, *Quantum Electrodynamics*, vol. 4 of *Course of Theoretical Physics* (Pergamon Press, Oxford, 1982), ISBN 9780750633710.

[52] L. S. Brown and T. Kibble, Phys. Rev. **133**, A705 (1964).

[53] I. I. Goldman, Phys. Lett. **8**, 103 (1964).

[54] F. Ehlotzky, K. Krajewska, and J. Z. Kamiński, Reports on Progress in Physics **72**, 046401 (2009), URL https://doi.org/10.1088%2F0034-4885%2F72%2F4%2F046401.

[55] C. Harvey, T. Heinzl, and A. Ilderton, Phys. Rev. A **79**, 063407 (2009), 0903.4151.

[56] M. Boca and V. Florescu, Phys. Rev. A **80**, 053403 (2009).

[57] F. Mackenroth and A. Di Piazza, Phys. Rev. A **83**, 032106 (2011), 1010.6251.

[58] T. Heinzl, D. Seipt, and B. Kämpfer, Phys. Rev. A **81**, 022125 (2010), 0911.1622.

[59] J. S. Toll (1952), PhD thesis, Princeton (unpublished).

[60] H. R. Reiss, Journal of Mathematical Physics **3**, 59 (1962), URL https://doi.org/10.1063/1.1703787.

[61] T. Heinzl, A. Ilderton, and M. Marklund, Phys. Lett. B **692**, 250 (2010), 1002.4018.

[62] A. Titov, A. Otto, and B. Kämpfer, Eur. Phys. J. D **74**, 39 (2020), 1907.00643.

[63] V. Dinu, T. Heinzl, and A. Ilderton, Phys. Rev. D **86**, 085037 (2012), 1206.3957.

[64] T. W. B. Kibble, Phys. Rev. **138**, B740 (1965).

[65] T. W. B. Kibble, A. Salam, and J. A. Strathdee, Nucl. Phys. B **96**, 255 (1975).

[66] V. Dinu, Phys. Rev. A **87**, 052101 (2013), 1302.1513.

[67] A. Ilderton, Phys. Rev. D **101**, 016006 (2020), 1910.03012.

[68] A. Ilderton, B. King, and S. Tang, Phys. Lett. B **804**, 135410 (2020), 2002.04629.

[69] A. K. Khokonov, M. K. Khokonov, and A. A. Kizdermishov, Tech. Phys. **47**, 1413 (2002), [Zh. Tekh. Fiz. **47**, 69 (2002)].

[70] T. G. Blackburn, D. Seipt, S. S. Bulanov, and M. Marklund, Phys. Plasmas **25**, 083108 (2018), 1804.11085.

[71] V. Dinu and G. Torgrimsson, Phys. Rev. D **97**, 036021 (2018), 1711.04344.

[72] V. Dinu and G. Torgrimsson, Phys. Rev. D **99**, 096018 (2019), 1811.00451.

[73] K. Krajewska and J. Z. Kamiński, Phys. Rev. A **85**, 062102 (2012), URL https://link.aps.org/doi/10.1103/PhysRevA.85.062102.

[74] K. Krajewska and J. Z. Kamiński, Phys. Rev. A **86**, 052104 (2012), URL https://link.aps.org/doi/10.

1103/PhysRevA.86.052104.

[75] A. Angioi, F. Mackenroth, and A. Di Piazza, Phys. Rev. A **93**, 052102 (2016), URL https://link.aps.org/doi/10.1103/PhysRevA.93.052102.

[76] M. Babzien, I. Ben-Zvi, K. Kusche, I. V. Pavlishin, I. V. Pogorelsky, D. P. Siddons, V. Yakimenko, D. Cline, F. Zhou, T. Hirose, et al., Phys. Rev. Lett. **96**, 054802 (2006), URL https://link.aps.org/doi/10.1103/PhysRevLett.96.054802.

[77] V. I. Ritus, Nucl. Phys. B **44**, 236 (1972).

[78] A. Ilderton, Phys. Rev. Lett. **106**, 020404 (2011), 1011.4072.

[79] B. King and A. M. Fedotov, Phys. Rev. D **98**, 016005 (2018), 1801.07300.

[80] F. Mackenroth and A. Di Piazza, Phys. Rev. D **98**, 116002 (2018), 1805.01731.

[81] V. Dinu and G. Torgrimsson, Phys. Rev. D **101**, 056017 (2020), 1912.11017.

[82] U. Hernandez Acosta and B. Kämpfer, Plasma Phys. Control. Fusion **61**, 084011 (2019), 1901.08860.

[83] D. A. Morozov and V. I. Ritus, Nucl. Phys. B **86**, 309 (1975).

[84] E. Lötstedt and U. D. Jentschura, Phys. Rev. Lett. **103**, 110404 (2009), 0909.4984.

[85] D. Seipt and B. Kämpfer, Phys. Rev. D **85**, 101701 (2012), 1201.4045.

[86] F. Mackenroth and A. Di Piazza, Phys. Rev. Lett. **110**, 070402 (2013), 1208.3424.

[87] B. King, Phys. Rev. A **91**, 033415 (2015), 1410.5478.

[88] V. Dinu and G. Torgrimsson, Phys. Rev. D **99**, 096018 (2019), 1811.00451.

[89] V. P. Oleinik, Zh. Eksp. Teor. Fiz. **52**, 1049 (1967).

[90] K. Krajewska, Laser Phys. **21**, 1275 (2011), URL https://doi.org/10.1134/S1054660X11130172.

[91] A. Khokonov and M. Khokonov, Technical Physics Letters **31**, 154 (2005).

[92] V. Dinu, C. Harvey, A. Ilderton, M. Marklund, and G. Torgrimsson, Phys. Rev. Lett. **116**, 044801 (2016), 1512.04096.

[93] G. N. Watson, *A treatise on the theory of Bessel functions* (Cambridge University Press, 1995).